Submitted for publication in ApJ
Preprint typeset using LaTeX style emulateapj v. 12/16/11

A NEW METHOD TO ESTIMATE DARK MATTER HALO CONCENTRATIONS

Christian Poveda, Jaime E. Forero-Romero
Departamento de Física, Universidad de los Andes, Cra. 1 No. 18A-10, Edificio Ip, Bogotá, Colombia

Juan Carlos Muñoz-Cuartas
UdeA, Medellín, Colombia
Submitted for publication in ApJ

ABSTRACT

We present a new method to estimate the concentration of dark matter halos in N-body simulations. Our method is based on a fit to the integrated mass profile as a function of halo radius. The main advantage of this method is that it uses the full particle information without any binning. We test our method both on mock and N-body halos to compare it against two popular methods to find concentrations: maximum radial velocity measurements and radial particle binning to estimate the density. Tests on the mock halos show that the accuracy of our method to recover input concentrations varies with the number of particles in the halo. For halos sampled with 20 particles our method recovers the input concentration with 10% accuracy, while for the maximum radial velocity and density methods the accuracy is on the order of 20% and 100%, respectively. For halos samples with 10^4 particles our method achieves an accuracy of 0.01% while the velocity and density methods achieve 0.1% and 1% accuracy, respectively. We also measure the mass-concentration relationship on the N-body data. With respect to the other two approaches our method produces a flatter relationship, while its normalization falls below the maximum velocity method and above the density method.

Subject headings: methods: numerical — galaxies: halos — cosmology: theory — dark matter

1. INTRODUCTION

In the concordance cosmology paradigm the matter content of the Universe is dominated by dark matter, a collisionless fluid shaped by gravitational interactions. Simulations of dark matter dominated universes during the last three decades have provided valuable insights into the large scale structure formation process, showing a remarkable success when theoretical results are compared against observations of the galaxy distribution obtained from large surveys. (Springel et al. 2005; Klypin et al. 2011).

On galactic scales the most striking results of these simulations is that dark matter overdensities closely follow a universal density profile. In a first approximation this profile is spherically symmetric and its density only dependens on the radial coordinate. The universality of this profiles seems to be independent of the cosmological parameters and is self-similar for different spatial scales after an adequate re-scaling is applied. (Navarro et al. 1997; Taylor & Navarro 2001)

One the most popular parameterization for a dark matter halo radial density distribution is the Navarro-Frenk-White (NFW) profile (Navarro et al. 1997). This profile is a double power law in radius, where the transition break happens at the so-called scale radius r_s. The ratio between the scale radius and the virial radius R_v, which defines a natural scale for the halo, is known as the concentration $c = R_v/r_s$. Simulations show that the concentration is a strong function of halo mass and redshift.

High resolution simulations of Milky Way sized dark matter halos (Navarro et al. 2010) show that the universality property is not perfect and that a better fitting parameterization to the radial density profile is provided by the Einasto profile (Einasto 1965). However, the NFW density profile and its concentration have become a standard metric to describe the structure of dark matter halos.

Observationally, the relationship between halo mass and concentration could provide a potential test of LCDM on galactic scales. For this motivation a great deal of effort has been invested in calibrating this relationship with simulations (Neto et al. 2007; Duffy et al. 2008; Muñoz-Cuartas et al. 2011; Prada et al. 2012; Ludlow et al. 2014) and finding the best possible way to constraint it with observations (Buote et al. 2007; Comerford & Natarajan 2007; Mandelbaum et al. 2008; Giocoli et al. 2014; Foëx et al. 2014; Shan et al. 2015).

From the computational point of view there are two main methods to estimate the concentration parameter of a dark matter halo in a N-body simulation. The first method takes the particles composing the halos and bins them in logarithmic radii to estimate the density in each bin, then it proceeds with a fit of this density estimation as a function of the radius. A second method uses an analytic property of the NFW that relates the maximum of the ratio of the circular velocity to the virial velocity. The concentration can be then found as the root of an algorithmnic equation dependent on this maximum value.

The first method is straightforward to apply but presents two disadvantages. First, it requires a large number of particles in order to have a proper density estimate in each bin. This makes the method robust only for halos with at least 10^3 particles. The second

cn.poveda542@uniandes.edu.co
je.forero@uniandes.edu.co
xxx@udea.edu.co

problem is that there is not a way to estimate the optimal bin size, different choices produce different results for the concentration.

The second method solves the two problems mentioned above. It works with low particles numbers and does not involve data binning. However, it effectively takes into account only a single data point and discards the behaviour of the ratio $V_{\rm circ}/V_{\rm vir}$ below and above its maxima. Additionally, small fluctuations on the value of this maximum can yield large perturbations on the estimated concentration parameter.

In this paper we propose a new method to estimate the dark matter halo concentration in halos obtained in numerical simulations. It builds the cumulative mass profile from the particle data in the N-body simulation to find the best possible concentration value using a Markov Chain Monte Carlo (MCMC) methodology.

Our proposal has two advantages with respect to the two methods mentioned above. It does not involve data binning and does not throw away data points. Furthermore, the MCMC approach allows for an straightforward estimation of the uncertainties in the concentration parameter, and inclusion of informative priors.

2. BASIC PROPERTIES OF THE NFW DENSITY PROFILE

2.1. *Density profile*

The NFW density profile can be written as

$$\rho(r) = \frac{\rho_c \delta_c}{r/r_s(1+r/r_s)^2}, \tag{1}$$

where $\rho_c \equiv 3H^2/8\pi G$ is the Universe critical density, δ_c is the halo dimensionless characteristic density and r_s is the scale radius. This radius marks the transition between the power law scaling $\rho \propto r^{-1}$ for $r < r_s$ and $\rho \propto r^{-3}$ for $r > r_s$.

We define the virial radius of a halo, r_v, as the boundary of the spherical volume that encloses a density of Δ_h times the average density of the Universe. The corresponding mass M_v, the virial mass, can be written as $M_v = \frac{4\pi}{3}\bar{\rho}\Delta_h r_v^3$.

2.2. *Integrated Mass*

From these definitions we can compute the total mass enclosed inside a radius r:

$$M(<r) = 4\pi\rho_c\delta_c r_s^3 \left[\ln\left(\frac{r_s+r}{r_s}\right) - \frac{r}{r_s+r}\right]. \tag{2}$$

We express the same quantity in terms of dimensionless variables $x \equiv r/r_v$ and $m \equiv M(<r)/M_v$,

$$m(<x) = \frac{1}{A}\left[\ln\left(1+xc\right) - \left(\frac{xc}{xc+1}\right)\right], \tag{3}$$

where

$$A = \ln\left(1+c\right) - \left(\frac{c}{c+1}\right), \tag{4}$$

and the parameter c is known as the concentration $c \equiv r_v/r_s$.

From this normalization value and for later convenience we define the following function

$$f(x) = \ln\left(1+x\right) - \left(\frac{x}{x+1}\right). \tag{5}$$

The most interesting feature of Eq. (3) is that the concentration is the only free parameter to describe the density profile. In Figure 2 we show $m(<x)$ as a function of x for different values of the concentration in the range $1 \leq c \leq 20$.

2.3. *Circular velocity*

It is also customary to express the mass of the halo in terms of the circular velocity $V_c = \sqrt{GM(<r)/r}$. From this we can define a new dimensionless circular velocity $v(<x) \equiv V_c(<r)/V_c(<r_v)$, using the result in Eq. 3 to have:

In the right panel of Figure 2 we show the circular velocity profile for the same concentrations as in the left panel of Figure 2.

$$v(<x) = \sqrt{\frac{1}{A}\left[\frac{\ln\left(1+xc\right)}{x} - \frac{c}{xc+1}\right]}, \tag{6}$$

$$\frac{dv}{dx} = \frac{1}{A}\frac{\frac{2cx+1}{(cx+1)^2}cx - \log\left(cx+1\right)}{2x^2 v\left(x\right)} \tag{7}$$

this normalized profile always shows a maximum provided that the concentration is larger than $c > 2$. It is possible to show that for the NFW profile the maximum is provided by

$$\max(v(<x)) = \sqrt{\frac{c}{x_{\rm max}}\frac{f(x_{\rm max})}{f(c)}}, \tag{8}$$

where $x_{\rm max} = 2.163$ (Klypin et al. 2014) and the function $f(x)$ was defined in Eq. (5).

3. A NEW APPROACH TO ESTIMATE THE HALO CONCENTRATION

As we saw in the previous sections, once the density profile is expressed in dimensionless variables the only free parameter in the density profile is the concentration. There are two main methods to estimate concentrations in dark matter halos extracted from N-body simulations.

The first method tries to directly estimate the density profile. It takes all the particles in the halo and bins them in the logarithm of the radial coordinate from the halo center. Then, it estimates the density in each logarithmic bin counting the particles and dividing by the corresponding shell volume. At this point is is possible to make a direct fit to the density as a function of the radial coordinate. This method has been most recently used by Ludlow et al. (2014) to study the mass-concentration-redshift relation of dark matter halos using the Millennium Simulation Series.

A second method uses the circular velocity profile. As it was shown in the right panel of Figure (2) the circular velocity shows a maximum for all profiles with concentration values larger than $c > 2$. The method finds the value of x for which the normalized circular velocity $v(<x)$ shows a maximum. Using this value it solves numerically for the corresponding value of the concentration using Eq. (8). This method has been most recently used by Klypin et al. (2014) to study the mass-concentration-redshift relation using the Multidark Simulation Suite.

Our method is a third option that uses the integrated mass profile. First we define the center of the halo to

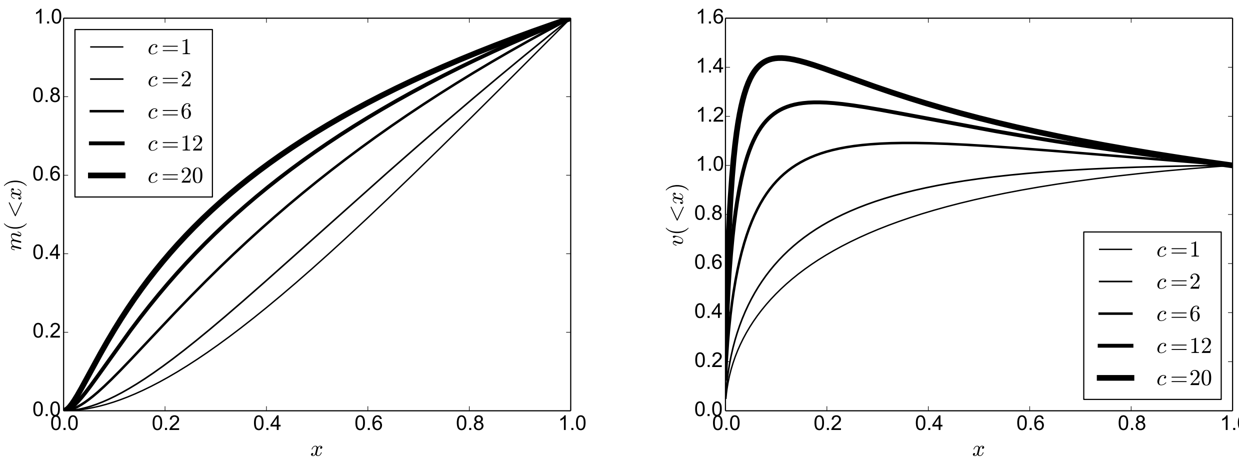

FIG. 1.— Dimensionless mass (left) and velocity (right) profiles as a function of the dimensionless radius for different concentration values.

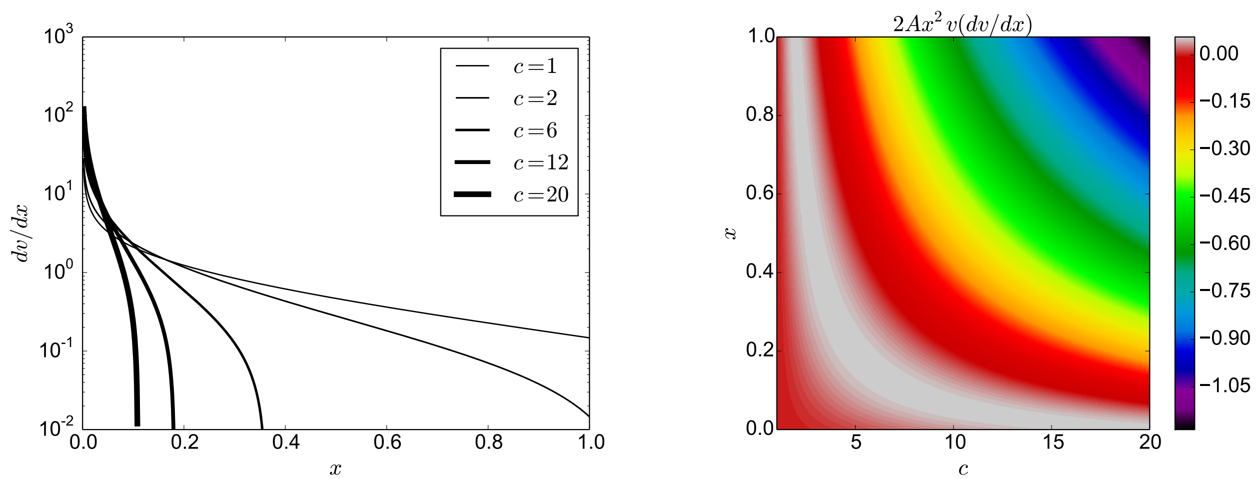

FIG. 2.— Dimensionless derivative of the velocity profile as a function of the dimensionless radius for different concentration values.

be at the position of the particle with the lowest gravitational potential. Then we rank the particles by their increasing radial distance from the center. From this ranked list of $i = 1, N$ particles, the total mass at a radius r_i is $M_i = i \times m_p$, where r_i is the position of the i-th particle and m_p is the mass of a single computational particle. In this process we discard the particle at the center.

We stop the construction of the integrated mass profile once we arrive at an average density of $\Delta_h\bar{\rho}$, with $\Delta_h = 740$, roughly corresponding to 200 times the critical density. This radius marks the virial radius and the virial mass. We divide the enclosed mass mass M_i and the radii r_i by these virial values to obtain the dimensionless variables m_i and x_i.

The construction of the numerical integrated mass profile has the advantage that it does not involve any binning and uses the information from all the particles in the halo, unlike the method that tries to directly build. Furthermore, as it will be clear in the next paragraph, the fit of this computational profile to the analytic expectation uses the information from all points, not only a single maxima point as the method using the circular velocity profile.

We use an Affine Invariant Markov chain Monte Carlo implemented in the python module emcee by FIXME (dfm et al) to sample the likelihood function distribution defined by $\mathcal{L}(c) = \exp(-\chi^2(c)/2)$ where the $\chi^2(c)$ is written as

$$\chi^2(c) = \sum_{i=1}^{N}[\log m_i - \log m(< x_i; c)]^2, \tag{9}$$

where $m(< x_i; c)$ corresponds to the values in Eq.(3) at $x = x_i$ for a given value of the concentration parameter c and the i index sums over all the particles in the numerical profile.

For the walk in the MCMC algorithm we used the default emcee parameters which are optimal. From the χ^2 distribution we find the optimal value of the concentration and its associated uncertainty.

4. RESULTS

In this Section we present the results of applying our method on two different halo samples.

The first sample is composed by mock halos generated to have known concentration values in perfect spherical symmetry following an NFW profile. We use this sample to check that we can recover the expected values but also gauge the impact of the number of particles on the outcomes and the difference with respect to the two other fitting methods.

The second sample comes from a publicly available N-body cosmological simulation. From this sample we quantify again the differences between all the methods we have to fit the data. We also estimate the possible impact of the different methods in estimating the mass-concentration relationship from simulations.

4.1. *Tests on Mock Halos*

The method we use to generate the halos is based on the integrated mass profile. We start by fixing the desired concentration c and total number of particles N in the mock halo. With these values we define the mass element as $\delta m = 1/M$, corresponding to the mass of each particle such that the total mass is one. Then for each particle, $i = 1, \dots, N$, we find the value of r_i such that the difference

$$m(< r_i; c) - i \cdot \delta m \qquad (10)$$

is zero using Ridders' method.

The value of r_i is the radius of the i-th particle of the mock halo. Then we generate random polar and azimuthal angles θ and ϕ for each particle to ensure spherical symmetry. Finally these three spherical coordinates are transformed into Cartesian coordinates $(r, \theta, \phi) \to (x, y, z)$.

We generate in total 400 mock halos split into four different groups of 100 halos each. The four groups differ in the total number of particles for their halos: 20, 200, 2000 and 20000. Inside each group the halos have random concentration values in the range $1 < c < 20$ with a uniform distribution. For all these halos with find the concentration values using the density, velocity and mass methods described in the previous section. We quantify the difference between the expected c_{in} and obtained c_{out} values by

$$D = (c_{in} - c_{out})/c_{in}. \qquad (11)$$

4.1.1. *The impact of particle number*

Figure 3 shows the integrated distribution for D for the fits using our method, split into four different groups according the particle number. From this Figure the first immediate conclusion is that increasing the number of particles increases the chances to recover the input values.

We believe that the main effect that contributes to this trend is that the particle that our algorithm finds to be the halo center (where the potential is minimum) gets closer to the original geometrical center (where no particle sits by construction) used to generate the halo. Poisson noise makes this center fluctuate, changing the numerical radial profile from the analytic input.

For particle number of 20 the offset between the input and output concentration can be as large as 20%, with

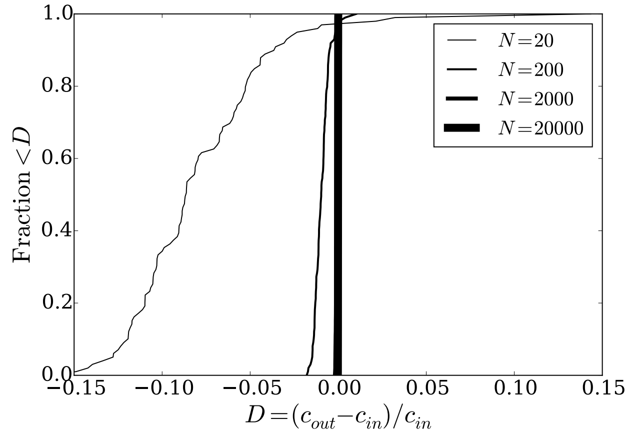

FIG. 3.— Cumulative distribution of the fractional difference, D, between the input concentration in the mock halo generator, c_{in} and the measurement by our MCMC code, c_{out}. Each curve corresponds to halos generated with a different number of particles, N.

a slight bias around −0.05%, i.e. the output concentration is biased towards lower values than the input. For particle numbers of 2000 most of the offsets fall below 5%, with a clear peak around 0% indicating that any appreciable bias is absent.

4.1.2. *The impact of the input concentration*

Figure 4 shows the integrared distribution for D for the fits using our method, split into different input concentrations for two different particle numbers describing the mock halos. On the left we have the case of halos sampled with $N = 20$ particles and on the right we have show results for halos with $N = 20000$ particles. The scale for D varies by almost three orders of magnitude. The accuracy of our method increases with larger values of N. This was already seen in the previous section. We explore the exact dependence of D with the number of particles in the next section when we compare the accuracy of different methods.

There are two interesting in Figure **??**. The first is that our method tends to underestimate the concentration and the second is that the degree of this underestimation increases with the input halo concentration.

4.1.3. *The accuracy of different methods*

Using this data-set we also compare our method against the other two methods described earlier: using shells to estimate the density as a function of radius and the maximum circular velocity method. In the first case we use the same MCMC algorithm we have in our method to fit the density profile. In the second method we simply follow the procedure described in Section 3

We quantify the accuracy of each method with the following statistic:

$$\langle |D| \rangle = \frac{1}{|\mathcal{H}_N|} \sum_{\mathcal{H}_N} |D|, \qquad (12)$$

where $\mathcal{H}_N$ corresponds to the set of haloes with N particles, D follows the definition in Eq. (11) and $|\mathcal{H}_n|$ is the number of haloes in $\mathcal{H}_n$.

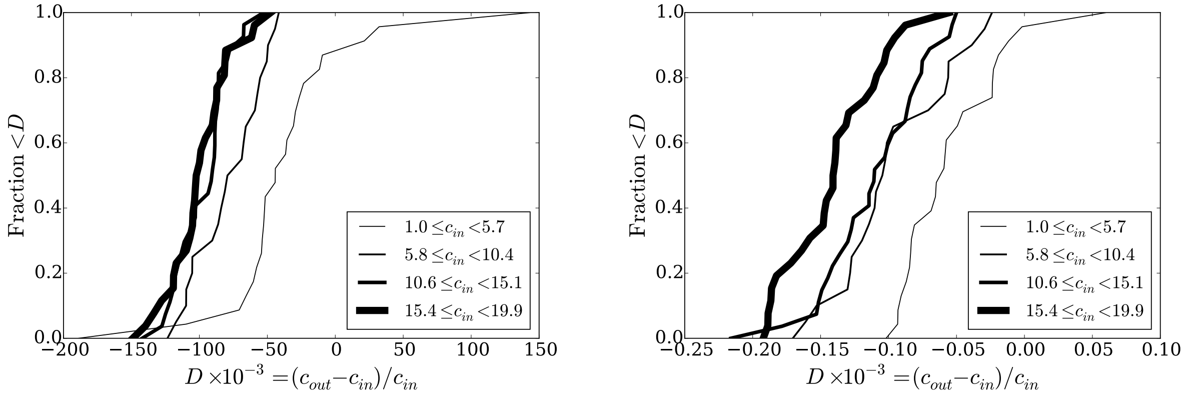

Fig. 4.— Cumulative distribution of the fractional difference, D, between the input concentration in the mock halo generator, c_{in} and the measurement by our MCMC code, c_{out}. Each curve corresponds to halos generated with an input concentration in a different range for a number of particles $N = 20$ (right panel) and $N = 20000$ (left panel).

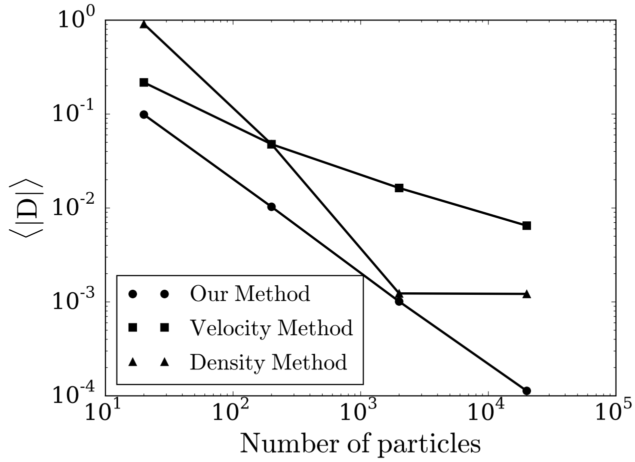

Fig. 5.— Average value of the relative error in the concentration estimate, $\langle |D| \rangle$, as a function of the particle number N in the set of mock halos. Different symbols represent different methods. Our method provide the most accurate estimate at fixed particle number N.

Figure 5 shows the behaviour of $\langle |D| \rangle$ as a function of halo particle number for the three different methods to estimate the concentration.

At fixed particle numbers our method almost always shows the lowest $\langle |D| \rangle$ values compared to the other two methods. Its accuracy is on the order of 10% for 20 particles in the halo, going down to 0.1% for halos with 20000 particles. The decrease of $\langle |D| \rangle$ with increasing particle number N goes approximately as $\langle |D| \rangle \propto N^{-1/2}$, which reinforces the hint that the accuracy of the method is related to a decrease of Poisson noise.

The method based on the maximum of the circular velocity shows a similar behaviour $\langle |D| \rangle \propto N^{-1/2}$. Its accuracy is $2-5$ times less than in our method, on the order of 20% for 20 particle halos and 0.5% for 20000 particle halos. The method based on the direct density fit shows the lowest accuracy for a low particle number and an intermediate accuracy between the other two methods for a high particle number.

4.2. *Tests on N-body data*

We use data from a N-body cosmological simulation that follows the non non-linear evolution of a dark matter density field sampled with 512^3 particles over a cubic box of 400 h^{-1}Mpc on a side. This simulation was run with the public available version of the Gadget-2 code. The simulation uses a standard ΛCDM cosmology with values of $\Omega_m = 0.258$, $\Omega_\Lambda = 0.742$ and $h = 0.72$ for the matter density parameter, cosmological constant parameter and the reduce Hubble constant, respectively. With these parameters the mass of an individual simulation particle corresponds to $3.41 \times 10^{10} h^{-1}\mathrm{M}_\odot$.

descripcion del halo finder

descripcionde separacion por grado de relajacion.

describcion de los resultados Figure 6 shows the results that compare the concentration values in the simulated halos from the three different methods.

5. CONCLUSIONS

REFERENCES

Buote, D. A., Gastaldello, F., Humphrey, P. J., Zappacosta, L., Bullock, J. S., Brighenti, F., & Mathews, W. G. 2007, ApJ, 664, 123

Comerford, J. M., & Natarajan, P. 2007, MNRAS, 379, 190

Duffy, A. R., Schaye, J., Kay, S. T., & Dalla Vecchia, C. 2008, MNRAS, 390, L64

Einasto, J. 1965, Trudy Astrofizicheskogo Instituta Alma-Ata, 5, 87

Foëx, G., Motta, V., Jullo, E., Limousin, M., & Verdugo, T. 2014, A&A, 572, A19

Giocoli, C., Meneghetti, M., Metcalf, R. B., Ettori, S., & Moscardini, L. 2014, MNRAS, 440, 1899

Klypin, A., Yepes, G., Gottlober, S., Prada, F., & Hess, S. 2014, ArXiv e-prints

Klypin, A. A., Trujillo-Gomez, S., & Primack, J. 2011, ApJ, 740, 102

Ludlow, A. D., Navarro, J. F., Angulo, R. E., Boylan-Kolchin, M., Springel, V., Frenk, C., & White, S. D. M. 2014, MNRAS, 441, 378

Mandelbaum, R., Seljak, U., & Hirata, C. M. 2008, JCAP, 8, 6

Muñoz-Cuartas, J. C., Macciò, A. V., Gottlöber, S., & Dutton, A. A. 2011, MNRAS, 411, 584

Navarro, J. F., Frenk, C. S., & White, S. D. M. 1997, ApJ, 490, 493

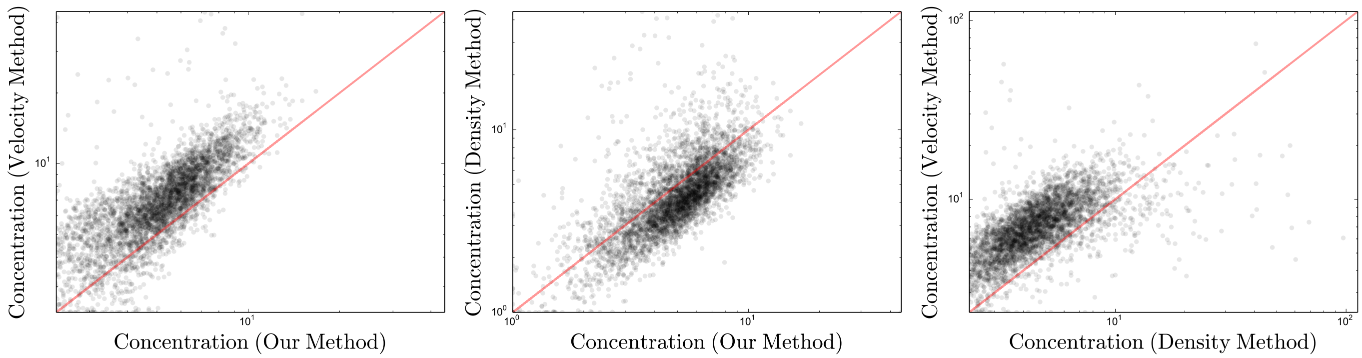

FIG. 6.— Comparison between the concentrations measured by our method and the maximum velocity (left) and density (middle) methods. The line indicates the equal value between the two techniques. The right panel compares the results of the maximum velocity and density methods.

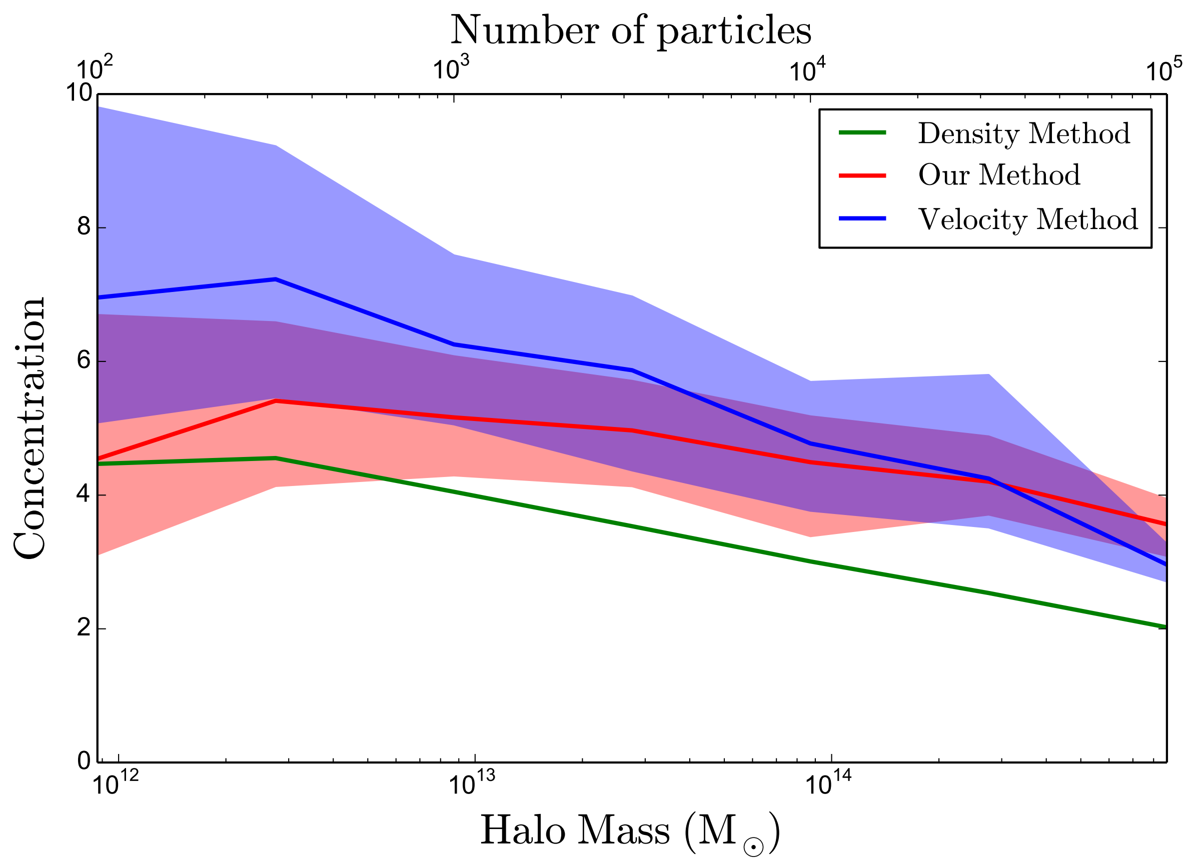

FIG. 7.— Mass-concentration relationship for the three different methods used on the same cosmological N-body data. The central lines correspond the median and the shadowed region indicates the quartiles.

Navarro, J. F., Ludlow, A., Springel, V., Wang, J., Vogelsberger, M., White, S. D. M., Jenkins, A., Frenk, C. S., & Helmi, A. 2010, MNRAS, 402, 21
Neto, A. F., Gao, L., Bett, P., Cole, S., Navarro, J. F., Frenk, C. S., White, S. D. M., Springel, V., & Jenkins, A. 2007, MNRAS, 381, 1450
Prada, F., Klypin, A. A., Cuesta, A. J., Betancort-Rijo, J. E., & Primack, J. 2012, MNRAS, 423, 3018
Shan, H., Kneib, J.-P., Li, R., Comparat, J., Erben, T., Makler, M., Moraes, B., Van Waerbeke, L., Taylor, J. E., & Charbonnier, A. 2015, ArXiv e-prints
Springel, V., White, S. D. M., Jenkins, A., Frenk, C. S., Yoshida, N., Gao, L., Navarro, J., Thacker, R., Croton, D., Helly, J., Peacock, J. A., Cole, S., Thomas, P., Couchman, H., Evrard, A., Colberg, J., & Pearce, F. 2005, Nature, 435, 629
Taylor, J. E., & Navarro, J. F. 2001, ApJ, 563, 483